Reinforced Concrete Cable Stayed Bridge Towers under Cyclic Lateral Load

Hajime Ohuchi

繰返し水平力を受ける鉄筋コンクリート斜張橋主塔

大内　一

概　要

斜張橋主塔は一般に長柱となり，幾何非線形の影響を受けやすい。これは自重に対するコンクリートのクリープ変形や，大地震を想定した水平力を受ける時無視出来なくなる。そこで橋軸直交方向水平力を受ける主塔に関し，一連のパラメトリック解析を実施し，特に，(1)耐力や変形能力に及ぼすクリープや水平繰返し荷重の影響，(2)幾何非線形に伴う付加モーメントに関する現行設計法（ACI 基準）の妥当性に着目して検討を加えた。その結果次のことが判った。① 柱の細長比（l/r）$\leqq 100$，自重による初期軸力（σ_0/f_c'）$\leqq 0.2$の範囲内では耐力，変形能力に及ぼすクリープや繰返し荷重の影響は少ない。② 付加モーメントに関する現行設計法（ACI 基準）は，応力再配分の影響の大きな小細長比の場合を除き安全側の評価を与える。③ 十分な変形能力を持たせるには，$\sigma_0/f_c' \leqq 0.1$とする。今後の研究課題として，コンクリートの拘束効果に関し軟化域までの調査が必要である。

Abstract

A series of static analyses up to failure are conducted with various parameters which govern the nonlinear behavior of an A-shaped cable stayed bridge tower, under sustained gravity load combined with seismic lateral load. The present study particularly focuses on the influence of creep deformation and of cyclic lateral load on the ultimate strength and the ductility of the tower and the applicability of the current 'Moment Magnifier Method' in the ACI code. Analytical results indicate that no significant effect of creep and cyclic load is observed on the ultimate strength behavior for towers in the range of slenderness ratios $l/r \leqq 100$ and having an axial stress due to gravity load $\sigma_0/f_c' \leqq 0.2$. The current moment magnifier method gives results on the conservative side except for the low slenderness ratio region in which considerable moment redistribution takes place due to axial force variation.

1. Introduction

For a column type structure such as a cable stayed bridge tower, reinforced concrete is cost effective with high compressive strength. However such towers may often have long columns and therefore some difficult design problems need to be resolved.

There have been many studies on the hysteretic characteristics of short columns under cyclic lateral loads. However, very few studies have been made on these characteristics for a slender column. Geometric nonlinearity may have an effect even on ultimate load capacity and ductility. Under high axial load, secondary moments in columns increase due to additional creep deformation in the service load condition. The addition of lateral earthquake load may lead to a further influence of this secondary moment.

The Moment Magnifier Method[1] has been widely used in the design of slender columns. This method was proposed by J. E. Breen et al.[2),3)] based on experiments on columns and box type frames under monotonic axial loads with eccentricity. No axial load variation was considered in these experiments and in that sense, the above design equation is only applicable for a single column with no axial force variation.

The present study investigates the influences of creep deformation due to gravity load and of cyclic lateral load on the ultimate strength and ductility. Also the applicability of the current ACI 'Moment Magnifier Method' to the analysis and design of a bridge tower subjected to transverse lateral loads is investigated with considering various parameters.

A detailed description of this study is given in the research report by Ohuchi.[4)]

2. Analytical Method

The analyses were carried out updating a nonlinear geometric, material and time dependent analysis computer program called 'PCFRAME' based on a comprehensive Ph. d. research study by Y. J. Kang[5)] at the University of California at Berkeley.

The analysis is based on the incremental form of the

displacement formulation of the finite element method. Nonlinear geometric effects are accounted for by a nonlinear term in the strain formulation and by continuously updating the nodal point geometry. Time dependent load history is considered using a step forward integration approach by dividing the time domain into a finite number of intervals.

Hognestad's stress-strain curve[6] is utilized for concrete with a straight descending part up to the ultimate strain ε_u. Unloading and reloading due to cyclic lateral load history is accounted for by a simple load reversal model with the initial tangent modulus E_i.

Total creep strain at any time t is numerically obtained as the sum of independent creep strains produced by stress changes at different loading times. In the present study, creep coefficients independent of age are assumed based on 28 days material constants.

A bilinear stress-strain model symmetrical about the origin, is assumed for the monotonic loading history of steel bars. The unloading path for stresses of both signs follows the initial elastic slope. After the first yield excursion the loading part of the stress-strain curve is represented by a Ramberg-Osgood relationship[6]. Good agreement was obtained for the cyclic moment-curvature relationship of an RC member in comparison between the present computer program and Park's analysis with Aoyama's experimental resuls[6]. The applicability of the present computer program to a slender column with creep deformation was verified in a comparison with column test[7] under eccentric axial load.

3. Analytical Models and Parameters

A frame type tower is very effective for satisfying lateral and torsional stiffness requirements in strong seismic zones.

An A-shaped reinforced concrete 400ft height tower with a uniform solid rectangular cross section is employed in the present study as shown in the Fig. 1. However, the results later discussed in nondimensional form can be applicable for other dimensions. It is reported[8] that usage of hollow section piers increases dramatically with height over 100 ft. Poston et. al.[9] also indicated that the assumption of plane sections remaining plane appears to be completely valid except for cases with very thin walls. Therefore, the results of the present study based on cross section constants such as flexural stiffness EI and slenderness ratio l/r, should be generally applicable for columns with any type of cross section in which a r expresses radius of gyration. A fixed support condition at tower base is chosen based on its advantage in design and construction aspects.[10]

The following factors are chosen as analytical parameters: configuration factor W/H=0.2, 0.4 and 0.6 (Fig. 1), slenderness ratio l/r=35, 69, 104, 156 and 208, gross reinforcement ratio p_g=1.5 and 3.0%, gravity load or initial axial load σ_o/f_c'=0.1, 0.2, 0.4 and 0.6, concrete creep and lateral load application (monotonic or cyclic). An eccentricity effect are neglected based on the reasons that the gravity load eccentricity is generally quite small compared with the displacement due to lateral load. Dynamic load effect, shrinkage, thermal strain and age dependent concrete properties are also neglected for simplicity.

The slenderness ratio is one of the most important factors which affects the structural behavior of a slender column such as the legs of bridge tower in the present study. The practical range of this factor l/r is considered to be from 40 to 80. For actual bridges constructed, l/r is about 45~70 for Pasco Kennewick[11], about 75 for East Huntington[12] and about 70 for James River bridge[13]. It is of importance to investigate its limitation for economical usage.

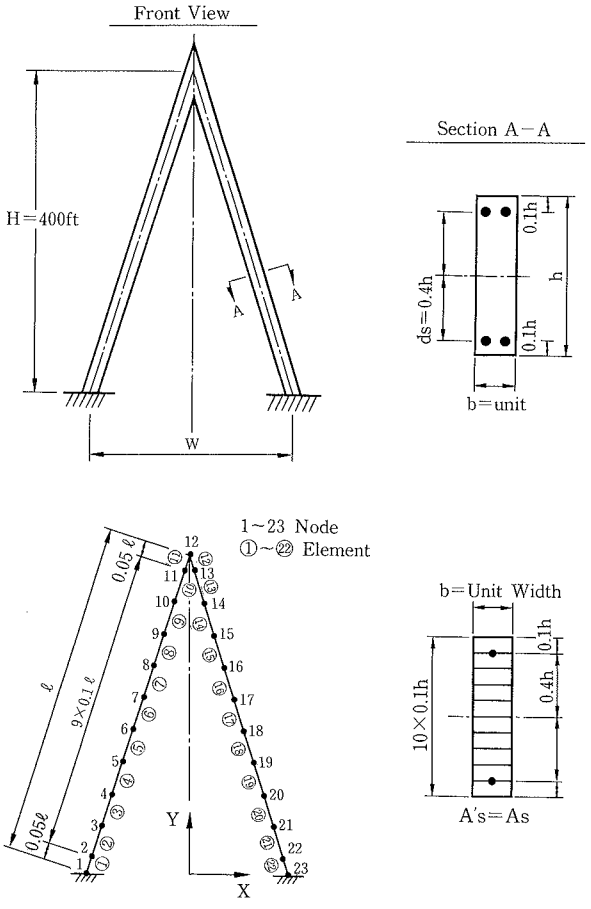

Fig. 1 Modelling of an A-Shaped Tower into Finite Elements and of Cross Section into Layers

Reinforcement ratios used in this study are in the practical range with reference to the existing Pasco Kennewick bridge with 1.5 to 2% and the test models with 1.27 and 2.25% by Ristic et. al.[14] for seismic safety investigation of a cable stayed bridge tower.

Material constants utilized in the present analysis are as follows. For concrete: $f_c'=6000$ psi (422 kg/cm^2), $E_i=33w^{1.5}\sqrt{f_c'}=4.42\times10^6$ psi (3.1×10^5 kg/cm^2) (w=1441b/ft^3: unit weight), $\varepsilon_u=0.0038$, $f_t'=7.5\sqrt{f_c'}=581$ psi (41 kg/cm^2), for concrete creep: $\lambda_i=10^{-1}(i=1,2,3)$, $a_1(t')=a_2(t')=0.1586\times10^{-6}$, $a_3(t')=0.1359\times10^{-6}$ ($c(t',t-t')=\sum_{i=1}^{3}a_i(t')[1-e^{-\lambda_i(t-t')}]$: creep function), and for rebar: $f_y=60$ ksi(4220 kg/cm^2)(Grade 60 steel bar), $E_s=29000$ ksi (2.04×10^6 kg/cm^2)($\therefore \varepsilon_{sy}=0.00207$), $E_s'=290$ ksi(2.04×10^4 kg/cm^2) for monotonic loading and 0 for cyclic loading, where E_s' is the strain hardening modulus of steel rebar.

4. Applied Loads and Load Combinations

Cable support arrangements distributions are different dependent on the cable stayed systems used. Dead and live load from girders including tower dead load itself are assumed to act together on the tower top as a vertical concentrated gravity load. This assumption should lead to a conservative solution with a greater geometric nonlinearity effect.

The structural behavior of a tower under seismic lateral loads perpendicular to longitudinal axis is conservatively assumed to have no interaction between the tower, supporting cables and girders. This lateral load distribution over the height of the tower is determined based on an first displacement mode in an elastic modal analysis using the SAP 80 computer program[15] for each tower with specific configuration and slenderness ratio. The distribution of this elastic lateral load is assumed to remain unchanged even in the nonlinear range. However, the magnitude of the load is increased proportionally and incrementally after the gravity load application. Three types of load combinations are employed for comparisons.

(1) Short term gravity load + monotonic increasing lateral load (S+H) neglecting time dependent effect.

(2) Long term gravity load + monotonic increasing lateral load (L+H): gravity load itself does not vary but internal force due to concrete creep.

(3) Long term gravity load + Cyclic lateral load (L+C. H).

Comparisons between (1) and (2) and between (2) and (3) are respectively for creep effects and for cyclic load effects from the elastic up to the ultimate range.

5. Monotonic Lateral Load Behavior

It is important to study the monotonic lateral load behavior with no creep effect to understand the basic behavior and also for later comparisons with other load combination cases. A total of 120 cases are analyzed with the various parameters previously described. In addition, a total of 45 cases with 3% rebar ratio are analyzed neglecting geometric nonlinearity for evaluation of this effect on the ultimate strength.

The observed failure modes as an entire structure are categorized in Table. 1. A creation of an 'Yield Hinge' is defined by a tensile yielding of rebar. The buckling failure modes Rank B' and EB' are separately defined because of their combination with a pinching mode which is the result of the negative overturning moment due to the concentrated gravity load at the top which tends to cancel the moment due to the lateral load. This was observed especially for a high gravity load case with a very slender column. This phenomena will be also described later.

In the numerical solution, buckling is defined when deformation suddenly increases without any appearance

Table 1 Failure Mode

● : Yield Hinge × : Concrete Crush

Rank	Failure Mode
1	
2	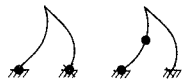
3	
B	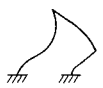 Inelastic Buckling
EB	 Elastic Buckling
B'	 Inelastic Buckling with Pinching Mode
EB'	 Elastic Buckling with Pinching Mode

of yielding or crushing under fairly small load increments intentionally applied.

In the Table. 2 failure mode ranks are tabulated for 120 cases under the S+H load combination. In the practical range of slenderness ratios less than 104, the cases of gravity load of σ_0/f_c' less than 0.2 indicate Rank 1 mode in general, but some of them Rank 2 mode because of being critical in concrete compression, especially for rebar ratio of $p_g=3\%$. In the range of slenderness ratio larger than 156, buckling failures occur even with low gravity load, particularly elastic buckling with high gravity load. Failure mode rank shown as $1 \rightarrow B$ or $2 \rightarrow B$ is the final buckling failure after reaching the mechanism 1 or 2. In general, it can be said that a ductile failure does not occur for a gravity load of σ_0/f_c' larger than 0.2 and that no significant differences of failure mode occur between different configuration factors and between different rebar ratios.

Some examples of ultimate strength ratio (τ_U/τ_U^0) vs slenderness ratio (l/r) relations are represented in Fig. 2 based on comparison between material, geometric nonlinear and only material nonlinear analyses, where τ_U is an ultimate strength due to the former and τ_U^0 due to the latter analysis. The greater the gravity load becomes, the more the reduction of this value appears (Fig. 2). Slightly less reduction is observed for smaller configuration factor, but no significant differences among these values. In the case of $\sigma_0/f_c'=0.6$ and $l/r=208$, a larger value is unexpectedly obtained because of the negative overturning moment action by a concentrated gravity load previously explained for the pinching mode case (Fig. 3 (a) pinching, (b) normal).

In general, the influence of geometric nonlinearity appears in the range of l/r larger than 69 for the larger gravity load, and 104 for the smaller gravity load (Fig. 2).

Table 2 Failure Mode Ranks of an A-Shaped Tower under Monotonic Lateral Load Combined with Short Term Gravity Load (S+H)

Rebar Ratio : $p_g=1.5\%$

Configuration Factor W/H	Slenderness Ratio		Axial Stress due to Gravity Load σ_0/f_c'			
	ℓ/h	ℓ/r	0.1	0.2	0.4	0.6
0.2	10	35	1	2	2	3
	20	69	1	2	2	3
	30	104	1	1	3	3
	45	156	2→B	B	B	EB
	60	206	B	B	B′	EB′
0.4	10	35	1	1	2	3
	20	69	1	1	3	3
	30	104	1	1	3	3
	45	156	1→B	B	B	EB
	60	208	B	B	B′	B′
0.6	10	35	1	1	2	3
	20	69	1	1	3	3
	30	104	1	1	3	3
	45	156	2→B	2→B	B	EB
	60	208	2→B	B	B′	EB′

Rebar Ratio : $p_g=3.0\%$

Configuration Factor W/H	Slenderness Ratio		Axial Stress due to Gravity Load σ_0/f_c'			
	ℓ/h	ℓ/r	0.1	0.2	0.4	0.6
0.2	10	35	2	2	3	3
	20	69	1	2	2	3
	30	104	2	2	3	3
	45	156	2	2	B	EB
	60	208	2→B	B	EB	B′
0.4	10	35	1	2	2	3
	20	69	1	2	3	3
	30	104	1	2	3	3
	45	156	1→B	2	B	EB
	60	208	2→B	B	EB	B′
0.6	10	35	1	2	2	3
	20	69	1	2	3	3
	30	104	1	2	3	3
	45	156	2→B	1	B	EB
	60	208	2→B	B	EB	B′

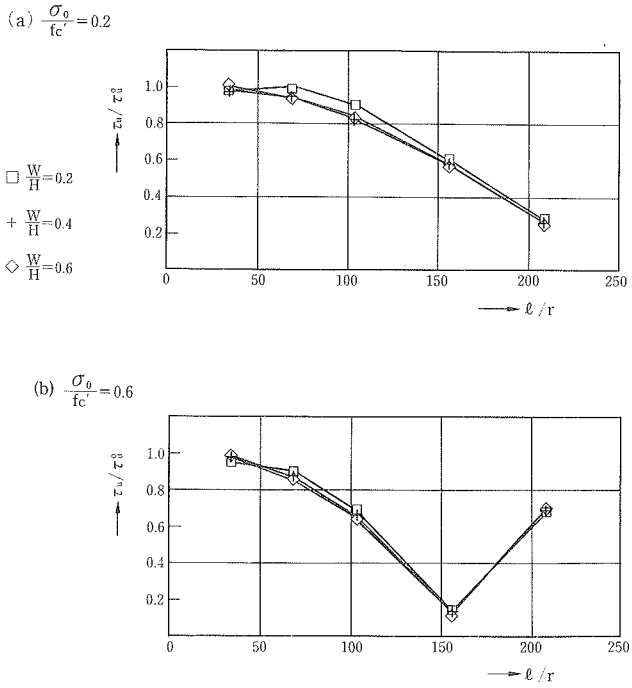

Fig. 2 Ultimate Strength Ratio Affected by Geometric Nonlinearity (Pg=3%)

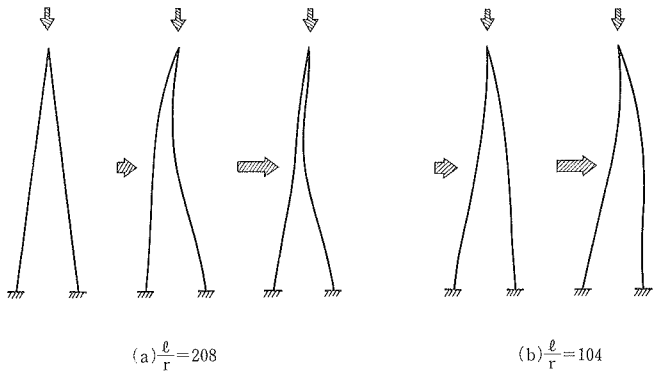

Fig. 3 Deformation Mode (W/H=0.2 $\sigma o/f'_c=0.6$ $P_g=3\%$)

A pair of examples of normalized ultimate strength vs. slenderness ratio relationships are shown in Fig. 4 with the vertical axis as a maximum average shear stress at base section divided by a conventional uni-axial compressive strength of concrete. With increase of configuration factor W/H, the value becomes large because of larger overturning moment resistance. However, similar results are observed among these values for l/r larger than 104 because of less variation of axial force existance. In other words the contribution of axial force diminishes in that l/r region. In the larger gravity load case, a more brittle failure tends to occur even in the small l/r region less than 104.

Ductility factor which is defined as the displacement at maximum load divided by that at first yielding of rebar, is shown in Fig. 5. The case in which tensile yielding of rebar is not reached is assigned as zero ductility for convenience. As the gravity load level or the slenderness ratio is increased, the ductility factor becomes smaller, but no significant differences are observed between configuration factors. In the low gravity load and small slenderness region, larger ductility is expected due to the creation of yield hinges.

6. Creep Effect

Comparisons between S+H and L+H Load cases for W/H=0.4 are shown in Table. 3. Both cases provide similar ultimate strength except for large gravity load and large slenderness ratio ranges. Under the creep deformation which occurs, the concrete is unloaded back to the elastic state. Therefore, the initial stiffness becomes larger but is followed by a considerable stiffness reduction due to the crack occurence in the earlier lateral load stage. As a result, the secondary moment increases and a lower ultimate strength is reached. On the contrary in the most severe case with $\sigma_0/f_c'=0.6$ and $l/r=156$, larger values are obtained because a larger elastic stiffness can be maintained up to buckling failure without any crack occurence.

For ductility factor, slightly reduced values, with at most 20% are observed. One reason is that the yield displacement of L+H case tends to be larger than that of S+H case. Another reason is that some errors are possibly involved to predict the maximum displacement in the numerical solution. A ductility factor less than one is not presented as no yielding of tensile rebar exists.

Failure modes are almost similar between L+H and S+H cases. They tend to be slightly more brittle in the smaller slenderness ratio region less than 104, but less in the larger l/r region.

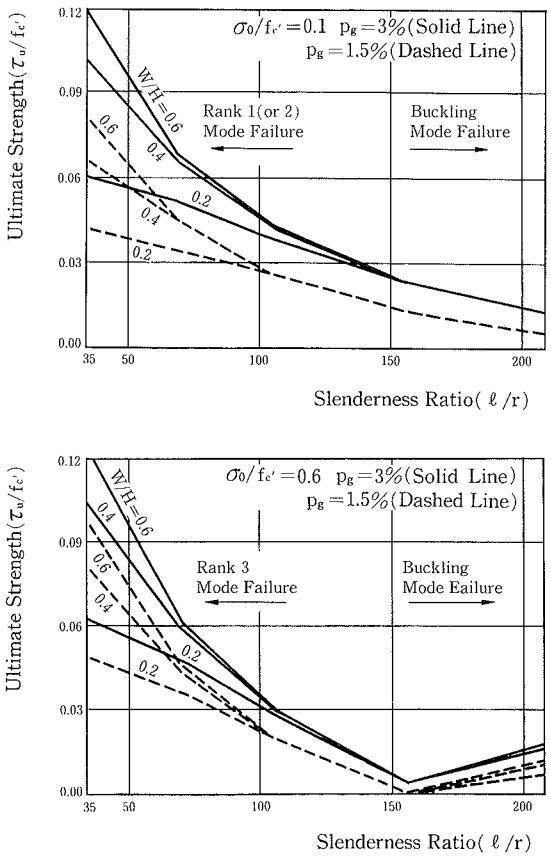

Fig. 4 Ultimate Strength-Slenderness Ratio Relationship

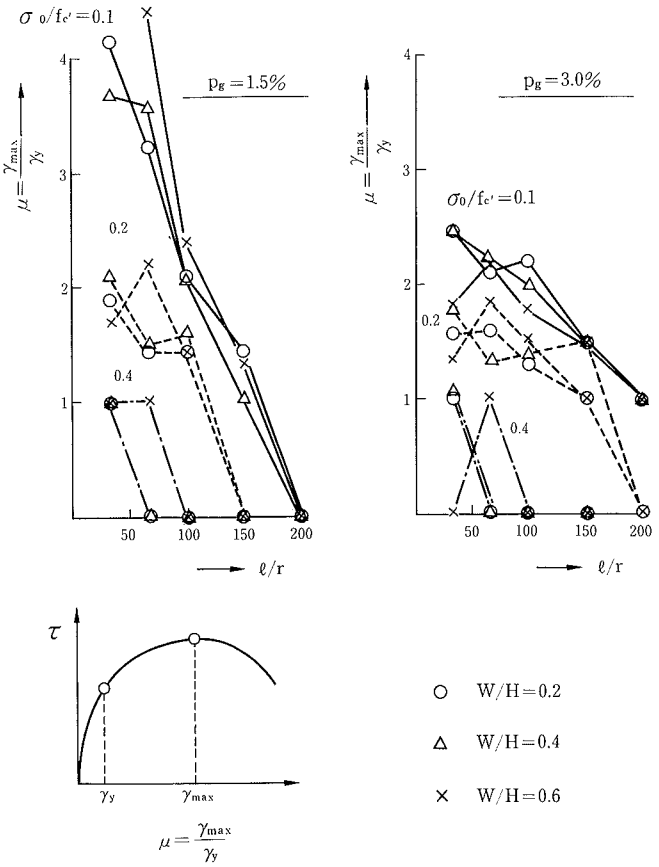

Fig. 5 Ductility Factor-Slenderness Ratio Relationship

Table 3 Ultimate States of an A-Shaped Tower Under Monotonic Lateral Load Combined with Long Term Gravity Load (L+H)

Rebar Ratio p_g	Config. Factor W/H	Axial Stress for G.L. σ_0/f_c'	Slenderness Ratio ℓ/h	Slenderness Ratio ℓ/r	Failure Mode Rank *1) S+H	Failure Mode Rank L+H	Ultimate Strength $\frac{\tau_u}{f_c'}$	Ultimate Strength *2) $\frac{\tau_u}{\tau_u^0}$	Ductility Facttor μ	Ductility Facttor *3) $\frac{\mu}{\mu^0}$
1.5%	0.4	0.1	10	35	1	1	0.0642	0.986	3.294	0.793
			30	104	1	1	0.0253	1.000	2.086	1.002
			45	156	1→B	1	0.0124	0.954	1.484	1.032
		0.2	10	35	1	2	0.0817	0.980	1.688	0.888
			30	104	1	2	0.0281	0.982	1.277	0.878
			45	156	B	B	0.0105	0.921		
		0.4	10	35	2	3	0.0901	0.956		
			30	104	3	3	0.0251	0.893		
			45	156	B	3→B	0.0071	0.941		
		0.6	10	35	3	3	0.0800	0.980		
			30	104	3	3	0.0170	0.829		
			45	156	EB	EB	0.0006	3.826		
3.0%		0.1	10	35	1	1	0.1001	0.993	2.220	0.897
			30	104	1	1	0.0426	0.988	1.762	0.795
			45	156	1→B	2	0.0234	0.975	1.333	0.902
		0.2	10	35	2	2	0.1101	1.000	1.536	0.974
			30	104	2	2	0.0411	0.976	1.269	0.971
			45	156	2	2	0.0195	0.963		
		0.4	10	35	2	3	0.1109	0.950		
			30	104	3	3	0.0366	0.913		
			45	156	B	B	0.0102	0.850		
		0.6	10	35	3	3	0.0984	0.952		
			30	104	3	3	0.0256	0.823		
			45	156	EB	3→B	0.0048	1.123		

*1) Reference data:Failure mode rank under monotonic lateral load combined with short term gravity load(S+H)
*2) Ratio of ultimate strength under L+H Load to that under S+H Load
*3) Ratio of ductility factor under L+H Load to that under S+H Load

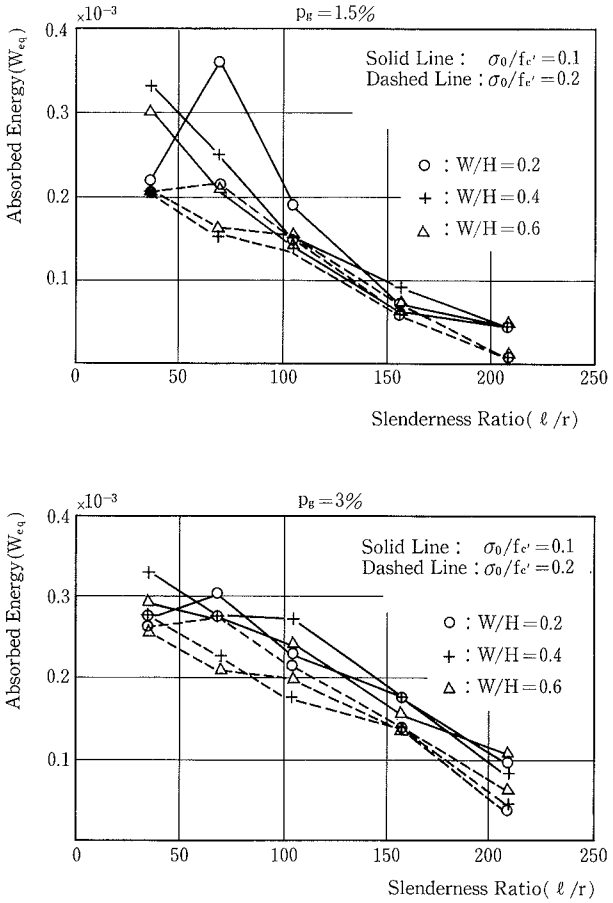

Fig. 6 Absorbed Energy-Slenderness Ratio Relationship

7. Absorbed Energy

Before discussing cyclic lateral load behavior, absorbed energy should be investigated based on the results for S+H load already presented with the purpose of excluding unnecessary analytical parameters. Fig. 6 shows the non-dimensional absorbed energy calculated by the area under the load-displacement curve up to the maximum load for the case of $\sigma_0/f_c'=0.1$ and 0.2 for which ductility design is considered to be possible. This absorbed energy is defined as an integrated external work by applied nodal forces. A representative displacement δ_{eq} is introduced by considering an equivalence with an external work.

$$\Delta W=\Sigma P_i\Delta\delta_i=(\Sigma P_i)\Delta\delta_{eq} \quad \cdots\cdots(1)$$

$$\therefore \Delta\delta_{eq}=\Sigma P_i\Delta\delta_i/\Sigma P_i \quad \cdots\cdots(2)$$

where P_i, $\Delta\delta_i$ are respectively a nodal force and an incremental nodal displacement, and the symbol Σ expresses summation through legs.

Non-dimensional expressions with an average shear stress at bottom leg section divided by f_c' and with a displacement divided by the tower height H make it possible to discuss for general dimensions of towers.

$$\Delta\gamma_{eq}=\Delta\delta_{eq}/H=\Sigma P_i\Delta\delta_i/H\Sigma P_i \quad \cdots\cdots(3)$$

Accordingly non-dimensional form of absorbed energy is given as follows.

$$W_{eq}=\int(\tau/f_c')d\gamma_{eq} \quad \cdots\cdots(4)$$

As shown in Fig. 6 top, the small reinforcement ratio case with $\sigma_0/f_c'=0.1$ provides a larger absorbed energy in the smaller slenderness ratio region dependent on the fair amount of plastic deformation accumulated in the yield hinges under an action of tensile axial force. Only exception is the W/H=0.2 and $l/r=35$ case in which the opposite bottom leg section (Elem-22, Fig. 1) becomes critical in axial compression. The larger axial load case (dashed line), meanwhile provides a rather smaller value due to smaller ductility despite the larger ultimate strength obtained. On the other hand, in the case of larger reinforcement ratio as shown in Fig. 6 bottom, a larger value than the former case is obtained in the entire region, but is apparently limited by the concrete failure particularly in the smaller l/r region.

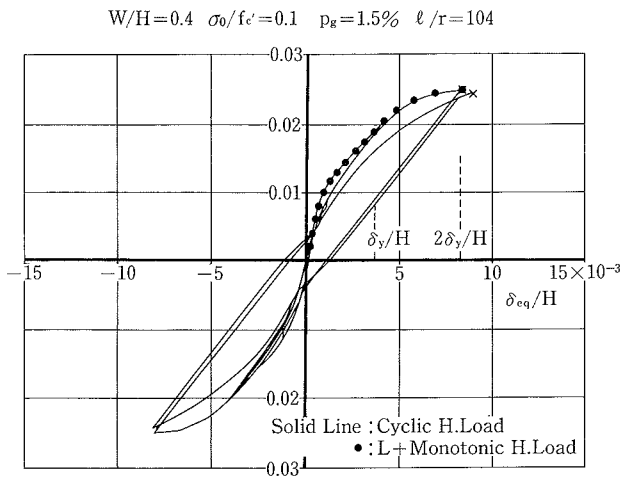

Fig. 7 Load-Displacement Relationship (Equivalent Displacement)

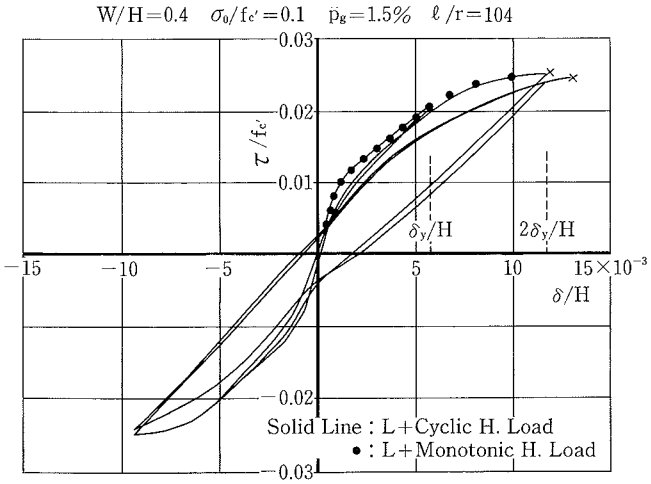

Fig. 8 Load-Displacement Relationship (Node-7)

8. Cyclic Lateral Load Behavior

Based on the preceding discussions, the follwing parameters are adopted for the cyclic load analyses (L+C.H) : W/H=0.4, p_g=1.5 and 3.0%, l/r=35 and 104. A displacement control type load application is conducted based on the yield displacement, δ^{y}_{eq} with two cycles at each displacement level for the 1.5% reinforcement ratio series, and with only one cycle for the 3% series because no influence of a cyclic number was found through former series.

In the Fig. 7 and 8, examples of load-displacement relations are shown regarding the equivalent (eq. (3)) and the midpart (Node-7, Fig. 1) displacement. Despite the lack of ductility with failure shortly after the 2 δ_y loading cycle, a comparatively good capability in absorbed energy appears. The skelton curve including the ultimate strength and the ductility corresponds to the monotonic loading case. An unsymmetric relationship of the midpart displacement is obtained for positive and negative loading as shown in Fig. 8 since the column member has a different stiffness between tensile and compressive axial force application.

The failure mode, the ultimate strength and ductility by cyclic lateral load analyses are tabulated in the Table. 4. As shown, the ultimate strength reduction is within at most 5% in comparison with the monotonic loading result. The ductility factor provides a slightly larger value than monotonic loading case for p_g1.5% and at most 3% less for p_g=3%. Failure modes generally show similar results, with the only difference of Rank 2 failure mode for the p_g=1.5% and σ_0/f_c'=0.2 case.

It is of interest to investigate the overturning moment variation due to geometric change. Fig. 9

Table 4 Ultimate States of an A-Shaped Tower under Cyclic Lateral Load Combined with Long Term Gravity Load (L+C. H)

Rebar Ratio p_g	Config. Factor W/H	Axial Stress for G.L. σ_0/f_c'	Slenderness Ratio ℓ/h	Slenderness Ratio ℓ/r	Failure Mode Rank *1) S+H	Failure Mode Rank L+C.H	Ultimate Strength $\frac{\tau_u}{f_c'}$	Ultimate Strength *2) $\frac{\tau_u}{\tau_u^0}$	Ductility Factor μ	Ductility Factor *3) $\frac{\mu}{\mu^0}$
1.5%	0.4	0.1	10	35	1	1	0.0626	0.962	4.222	1.017
			30	104	1	1	0.0246	0.972	2.343	1.126
		0.2	10	35	1	2	0.0817	0.980	2.096	1.103
			30	104	1	2	0.0276	0.965	1.532	1.054
3.0%		0.1	10	35	1	1	0.0959	0.951	2.452	0.991
			30	104	1	1	0.0421	0.977	2.197	0.992
		0.2	10	35	2	2	0.1068	0.970	1.721	1.091
			30	104	2	2	0.0401	0.952	1.270	0.972

*1) Refererce data:Failure mode rank under monotonic lateral load
*2) Ratio of ultimate strength under L+C. H Load to that under S+H Load
*3) Ratio of ductility factor under L+C. H Load to that under S+H Load

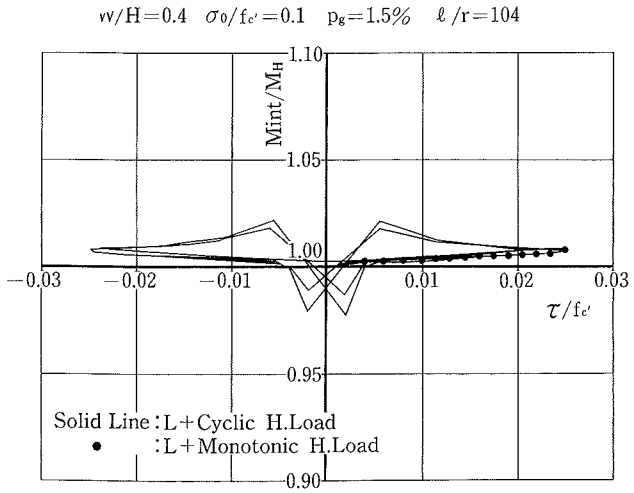

Fig. 9 Internal Moment-Load Relationship

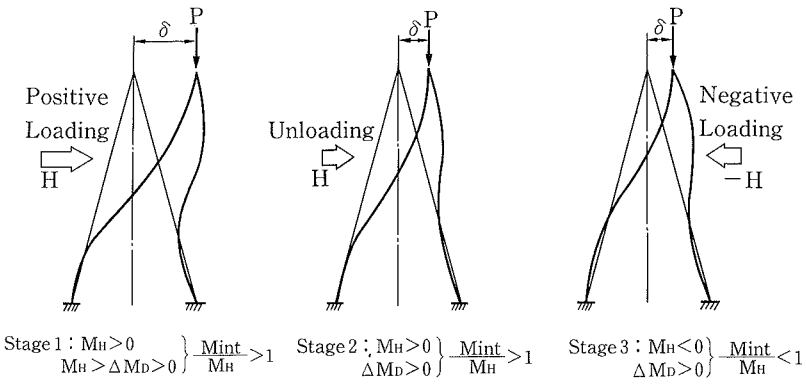

(a) Loading with Large H (b) Unloading with Small H (c) Negative Loading with Positive Residual Displacement

Fig. 10 Participation of Secondary External Moment

represents the internal moment variation under cyclic lateral load. M_{int} is the internal overturning moment at base calculated by internal nodal forces, while M_H is the external overturning moment at base based on initial geometry. Therefore, the deviation from unit value can be thought of as an external moment variation based on geometric change. As far as a convergent solution is obtained, an external moment should be equal to an internal moment.

During unloading, this value moves on the different path from loading path since the additional moment, $\Delta M_D = M_{int} - M_H$ due to geometric change including gravity load contribution becomes relatively larger in comparison with M_H because of the existence of residual deformation as shown in Fig. 10 (b). On the other hand, when negative loading starts, an additional moment ΔM_D remains positive with a negative first moment M_H (Fig. 10 (c)). Accordingly, the value of M_{int}/M_H becomes less than one in that region. Under the further negative lateral loading, the value is recovered to be larger than unit value on the normal loading path. This value, however remains in 1 or 2% deviation even during the maximum loading cycle and at most 2 to 3% deviation even during the transient region across the neutral.

9. Moment Magnification Factor

A typical stress path at a particular section under monotonic lateral load combined with gravity load is shown in Fig. 11, where the solid line shows a nonlinear stress path, while the dashed line linear path based on a conventional elastic analysis. (M_1, N_1) and (M_1^e, N_1^e) respectively corresponds to a nonlinear and a linear stress point under gravity load, and (M_2, N_2) and (M_2^e, N_2^e) under ultimate lateral load. In the present study, the stress point at failure is adopted as (M_2, N_2) whether it is monotonic or cyclic loading.

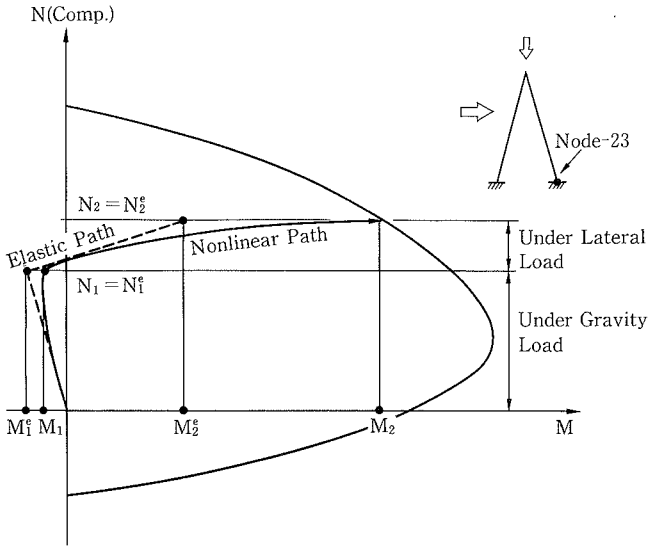

Fig. 11 A Typical Stress Path at the Bottom Leg Section (Node-23)

In the current design code[1], the moment magnification factor δ_b for a braced frame is specified by following equations.

$$\delta_b = C_m/(1-\Phi P_u/P_c) \geqq 1.0 \quad \cdots\cdots(5)$$

$$P_c = \pi^2 EI/(kl_u)^2 \quad \cdots\cdots(6)$$

In order to determine design moment magnification factor in the present study, following factors are adopted: $C_m=1$, $P_u=N_2$ (Fig. 11) and $k=0.625$, $l=l_u$ (full length of a leg) and EI are determined based on ACI code[16].

An analytical moment magnification factor is calculated by the following equation.

$$\delta_b^{anal} = M_2/M_2^e \quad \cdots\cdots(7)$$

In the present model, the gravity load moments, M_1 and M_1^e are both much smaller than combined moments M_2 and M_2^e. Therefore, M_2 and M_2^e almost equals to lateral load moment M_2-M_1 and $M_2^e-M_1^e$ respectively.

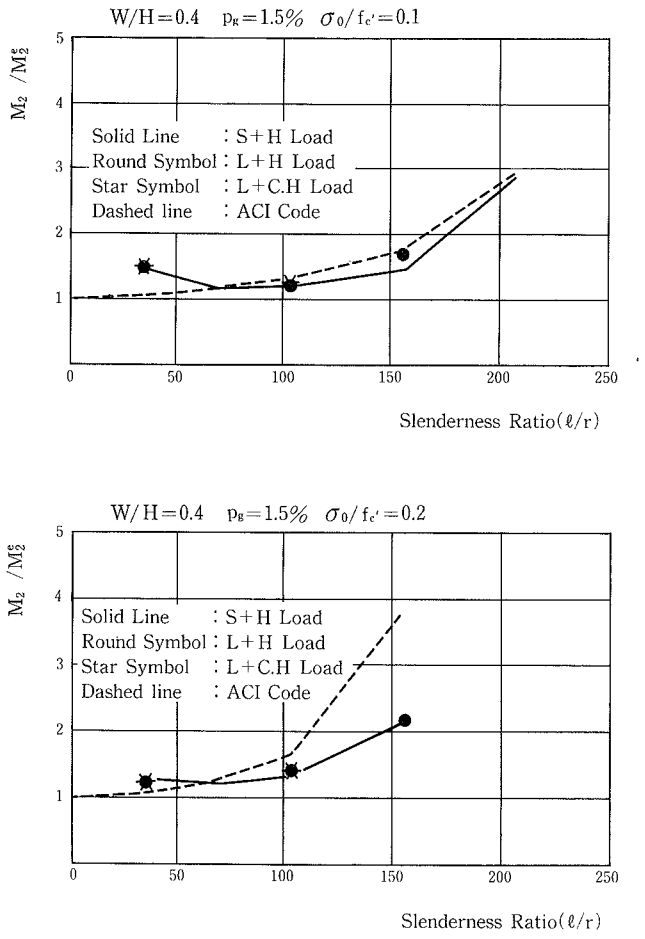

Fig. 12 Moment Magnification Factor-Slenderness Ratio (P_g=1.5%)

Fig. 12 shows the representative moment magnification factor for various load combination regarding Node-23 (Fig. 1) where the secondary moment is the largest through the structure. The result of cyclic load analyses (L+C. H) are not so different from another analytical cases. An analytical value at l/r=35 exists above the ACI design value because of the larger moment redistribution occuring between both legs. Except this region, the ACI design value is on the conservative side.

10. Conclusions

Based on the results presented, a number of important conclusions can be summarized as follows:

1. For l/r larger than 100, the resisting potential as an entire structure is poor. Especially for l/r larger than 150, a drastic sudden failure such as buckling could occur even under low gravity load.
2. The ductility and the absorbed energy defined as the displacement at and the area up to maximum load can decline dependent on the gravity load, the rebar ratio and the slenderness ratio. Design usage of gravity load σ_0/f_c' less than 0.1 and a slenderness ratio l/r less than 100 is recommended for ductility design performance with plastic hinges sufficiently created.
3. During a sustained gravity load due to creep, the concrete is unloaded in compression, while rebar has an increase in compression for compensation. As a result, a higher initial stiffness is recovered followed by the earlier stiffness reduction due to crack occurence in the early stage of lateral load. This stiffness reduction may cause the structure to be somewhat brittle. However the influence on both ultimate strength and ductility is small for σ_0/f_c' less than 0.2 and l/r less than 100 which include the above recommended ranges.
4. The cyclic load analyses considering creep effects indicate no significant influences of cyclic load on the ultimate strength and the ductility for a gravity load σ_0/f_c' less than 0.2 and a slenderness ratio l/r less than 100.
5. The moment magnification factor found in the present analytical study is larger than the ACI design value for a slenderness ratio l/r=35 with an axial load σ_0/f_c' less than 0.2 because of the moment redistribution occuring between both legs due to axial force variation. The current ACI design method, meanwhile generally provides a conservative value except in the above region. There are no significant influences of cyclic load and creep on this factor for σ_0/f_c' less than 0.2 and l/r less than 100 ranges.
6. Ductility factors investigated in the present study may give an underestimation because of the neglection of softening behavior. Future studies including the softening behavior range and the effects of concrete confinement are needed in this respect.

Acknowledgments

A major part of this study was carried out at the Department of Civil Engineering of the University of California at Berkeley during author's stay as a Visiting Scholar. The author wish to express his deepest appreciation and gratitude to the faculty investigator, Prof. A. C. Scordelis for his constant guidance and also to Prof. Y. J. Kang from Seoul University and Graduate Student K. Krishnan for their help and useful suggestions. The Computer Center at the University of California, Berkeley provided the facilities for the numerical work.

References

1) ACI : Building code requirement for reinforced concrete, 3rd printing, American Concrete Institute, (1985)
2) Breen, J. E. and Macgregor, J. G. : Determination of effective length factors for slender concrete columns, J. American Concrete Inst. Vol. 69, No. 63, P. 669-672, (1972)
3) Macgregor, J. G., Breen, J. E. and Phrang, E. O. : Design of slender concrete columns, J. American Concrete Inst., Vol. 67, No. 2, P. 6-28, (1970)
4) Ohuchi, H. : Nonlinear behavior of reinforced concrete cable stayed bridge towers under cyclic latelal load, SEMM Report No. 88-23, University of California, Berkeley, (1988)
5) Kang, Y. J. : Nonlinear geometric, material and time dependent analysis of reinforced and prestressed concrete frames, SESM Report No. 77-1, University of California, Berkeley, (1977)
6) Park, R. and Paulay, T. : Reinforced Concrete Structures, Wiley-Interscience Publication, John Wiley & Sons, New York, NY, (1975)
7) Hellesland, J., Choudhury, D. and Scordelis, A. C. : Nonlinear analysis and design of RC bridge columns subjected to imposed deformations, SESM Report No. 85-3, University of California, Berkeley, (1985)
8) Poston, R. W., Diaz, M. and Breen, J. E. : Design trend for concrete bridge piers, J. American Concrete Inst., Vol. 83 No. 2, P. 14-20, (1986)
9) Poston, R. W., Gilliam, T. E., Yamamoto, Y. and Breen, J. E. : Hollow concrete bridge pier behavior, J. American Concrete Inst., Vol. 82, No. 70, P. 779-787, (1985)
10) ASCE : Commentary on the tentative recommendations for cable stayed bridge structures, The task committee on cable-suspended structures, J. Struct. Div., ASCE. Vol. 103, No. 5, P. 941-959, (1977)
11) Grant, A. : The Pasco-Kennewick Intercity Bridge, J. Prestressed Concrete Inst., Vol. 24 No. 3, P. 90-124, (1979)
12) Grant, A. : Design and Construction of the East Huntington Bridge, J. Prestressed Concrete Inst., Vol. 32, No. 1, P. 20-29, (1987)
13) Robinson, R. : Cable stays catch on, Civil Engineering, Vol. 56 No. 6, ASCE, P. 58-61, (1986)
14) Ristic, D., Yamada, Y. and Iemura, H. : Stress-strain based modelling of hystretic structures under earthquake induced bending and varying axial loads, Research Report No. 86-ST-01, Kyoto University, (1986)
15) Wilson, E. L. : Use of a CP/M-Micro computer as a structural engineering workstation, Version 1, 7, Dept. of Civil Eng., University of California, Berkeley, (1982)
16) ACI : Commentary on Building Code Requirement for Reinforced Concrete (ACI 318-83), 3rd Printing, American Concrete Institute, (1985)